ACS APPLIED MATERIALS & INTERFACES

Research Article

www.acsami.org

High-Performing $LiMg_xCu_yCo_{1-x-y}O_2$ Cathode Material for Lithium Rechargeable Batteries

Chandrasekaran Nithya, Ramasamy Thirunakaran, Arumugam Sivashanmugam, and Sukumaran Gopukumar*

CSIR–Network Institutes of Solar Energy (CSIR–NISE), CSIR–Central Electrochemical Research Institute (CSIR–CECRI), Karaikudi, India –630 006.

ABSTRACT: Sustainable power requirements of multifarious portable electronic applications demand the development of high energy and high power density cathode materials for lithium ion batteries. This paper reports a method for rapid synthesis of a cobalt based layered cathode material doped with mixed dopants Cu and Mg. The cathode material exhibits ordered layered structure and delivers discharge capacity of ~200 mA h g^{-1} at 0.2*C* rate with high capacity retention of 88% over the investigated 100 cycles.

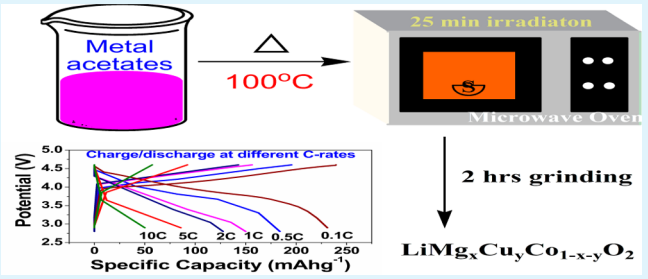

KEYWORDS: *acetate precursors, microwave method, layered oxides, doping, intercalation, galvanostatic cycling, cathode material*

1. INTRODUCTION

In the early 1990's, Sony Corporation successfully brought out the commercial lithium ion batteries. One of the most successful cathode materials for lithium ion batteries, lithium cobalt oxide, possesses the inherent drawback of low reversible capacity (~140 mA h g^{-1}), which eventually limits its storage capacity. Extensive research to explore new cathode materials has yielded lithium transition metal phosphates, which have lower voltage than $LiCoO_2$ and exhibit higher reversible capacity. This performance enhancement is achieved from nanosized particles and carbon coating.[1,2] The performance of $LiCoO_2$ can be improved by metal doping,[3] synthesis of nanosized particles and coating with inactive metal oxides.[4] Doping with transition metal cations Ti, Zr, Mg, Ni, Fe,[5−8] nontransition metal cations Al, Sn, Ga, etc.,[9−11] and rare earth metals[12] deliver high capacities up to 4.3 V, but fails beyond 4.3 V. The present day lithium ion batteries are normally charged upto 4.2 V and provide discharge capacity of 130−140 mA h g^{-1}. Increasing the charging voltage of lithium cobalt oxide based batteries to 4.3, 4.4, and 4.5 V Vs Li/Li^+ will significantly increases the reversible capacity to 160, 170, and 190 mA h g^{-1} respectively at 0.1*C* rate. Cho et al.[13] and other researchers have achieved high reversible capacities at high voltages through coating with inactive metal oxides which provide good structural stability during cycling. However, this approach involves time-consuming synthesis processes.

Ga has been suggested[11] as one of the effective dopants to improve the capacity of $LiCoO_2$ when cycled beyond 4.5 V. However, the capacity fades significantly upon cycling. Deepa et al. reported[14] that Cu−doping enhances conductivity of $LiCoO_2$ and M. Zou et al. stated[15] that Cu-doped $LiCoO_2$ exhibits better performance at 4.5 V with good capacity retention. On the other hand Mg-doping on $LiCoO_2$ is found to be beneficial in stabilizing the layered structure as reported by many authors.[16−18] The significance of increasing the charging voltage beyond 4.5 V can be achieved either by using suitable dopants to increase the conductivity, or by introducing a selective dopant to provide good structural stability at high voltages. This paper presents combining the benefits of dual doping (Cu and Mg) for increasing the structural and cycling stability of $LiCoO_2$ material up to 4.6 V, by rapid synthesis (25 minutes) using microwave heating.

2. EXPERIMENTAL SECTION

Synthesis of $LiMg_xCu_yCo_{1-x-y}O_2$, was carried out by mixing stoichiometric amounts of $Li(COOCH_3)_2{\cdot}2H_2O$, $Co(COOCH_3)_2{\cdot}4H_2O$, $Cu(NO_3)_2{\cdot}3H_2O$, and $Mg(COOCH_3)_2{\cdot}4H_2O$ and dissolving in minimum quantity of triple distilled water. The resulting solution was concentrated by stirring continuously at 100°C. Thus concentrated solution was transferred to a silica crucible and placed at the centre of the rotating plate of a microwave oven (Kenstar, India 2450 MHz, 800 W). The solution was irradiated at 100% power for 15−25 minutes. During the reaction, the acetates and nitrates were quickly burnt and a red glow appears inside the silica crucible throughout the reaction. After irradiation the product was ground for few hours to obtain phase pure $LiMg_xCu_yCo_{1-x-y}O_2$.

The synthesized product was characterized in an x−ray diffractometer ('Xpert PRO PANalytical PW 3040/60 'X'Pert PRO') at a scan rate of 1° min^{-1} using Cu−Kα radiation (λ = 1.5418A°), whereas the voltage and current were held at 40 kV and 20 mA (2θ = 0−80°). The surface morphology and microstructure of the synthesized samples were characterized in a scanning electron microscope (SEM HITACHI S−3000 H from Japan). Fourier transform infrared spectrum was recorded on a Nicolet 5DX − FTIR spectroscope

Received: May 13, 2012
Accepted: July 11, 2012
Published: July 11, 2012

dx.doi.org/10.1021/am300842x | *ACS Appl. Mater. Interfaces* 2012, 4, 4040−4046

using KBr pellet in the range of 400−2000 cm^{-1}. Room temperature Laser Raman spectra was recorded for the synthesized materials in a Renishaw InVia Laser Raman Microscope using the wavelength of 633 nm He−Ne laser. All spectra were recorded using an X-ray source (Al Ka radiation) with a scan range of 0−1200 eV binding energy and the workfunction of the spectrometer is 4.1 ± 0.1 eV. The collected high-resolution XPS spectra were analyzed using an XPS peak fitting software program. The energy scale was adjusted on the carbon peak in C1s spectra at 285 eV.

The cathode disc was prepared by mixing 80 wt % active materials, 10 wt % acetylene black, and 10 wt % polyvinylidene fluoride (PVDF) binder in N-methylpyrrolidone (NMP) solvent to form a homogeneous slurry. The mixture was coated over an aluminium foil and dried under ambient condition. 18 mm diameter circular discs were blanked out and dried under vacuum at 120 °C for 12h. Finally, coin cells of 2016 type were assembled inside an argon filled glove box using the above prepared cathode as working electrode, lithium as counter and reference electrode, celgard 2400 as the separator and $LiPF_6$ in 1:1 EC/DEC as electrolyte. Charge−discharge studies of the coin cells were carried out using a programmable battery tester at 0.1 and 0.2C rate for 50 cycles in the potential range of 2.7−4.6 V. Cyclic voltammetric measurements were performed using an EG&G instruments (Princeton Applied Research) at a scan rate of 0.1 mV s^{-1} between 2. 9 and 4. 6 V. Electrochemical Impedance Spectra were measured using an EG & G instruments Model 5210 with an AC voltage signal of 5 mV and frequency range between 100 kHz and 5 mHz.

3. RESULTS AND DISCUSSIONS

Figure 1a depicts XRD patterns of $LiMg_xCu_yCo_{1-x-y}O_2$ cathode materials synthesized by microwave method. All the diffraction patterns are indexed to hexagonal α-$NaFeO_2$ type layered structure having $R\bar{3}m$ space group confirming single phase formation. As can be seen from panels b and c in Figure 1, the splitting of peaks corresponding to planes (006), (102) and (108), (110) figures demonstrates that the formation of well ordered layered structure. The lattice parameters of the synthesized materials are calculated by using X'Pert Highscore plus software program and presented in Table 1. As Mg and Cu content increases, both 003 and 101 peaks slightly shift to lower angle, indicating that Mg and Cu doping enlarges lattice parameters along the '*a*' and '*c*' directions. This can be attributed to the larger ionic radius of Cu^{2+} and Mg^{2+} ions than Co^{3+} ion, which is in agreement with previous reports.[19,20] Further, variation in trigonal distortion (c/a ratio) also follows the same trend as the lattice parameters. The value of c/a ratio greater than 4.9 indicates the formation of ordered hexagonal layered structure.[21] The enlargements of lattice constants confirm the replacement of Co^{3+} ions by the Mg^{2+} ions.[22−24] In the XRD patterns of our products, the intensity ratio of the 003 and 104 peaks is less than 1.2, suggesting the possibility of undesirable cation mixing.[25,26] Generally, the cation mixing occurs because of partial interchange of Li and transition metal ions. This indicates that the electrochemical activity of the synthesized materials in terms of specific capacity and rate of Li extraction and insertion during cycling should be good as reported by Y. Makimura et al.[27] Further, an R factor ($R = ((I_{102} + I_{006})/I_{101})$ value of 0.39 to 0.53, an indicator of hexagonal ordering related to the integrated intensities of corresponding peaks, confirms the hexagonal ordering.

Figure 2 shows SEM images of $LiMg_xCu_yCo_{1-x-y}O_2$ materials synthesized by microwave method. All the particles are of submicrometer sizes in the range of 0.5−1 μm. The particles are generally agglomerated, and for the composition x = 0.005 and y = 0.195 the grains appear as irregular shaped

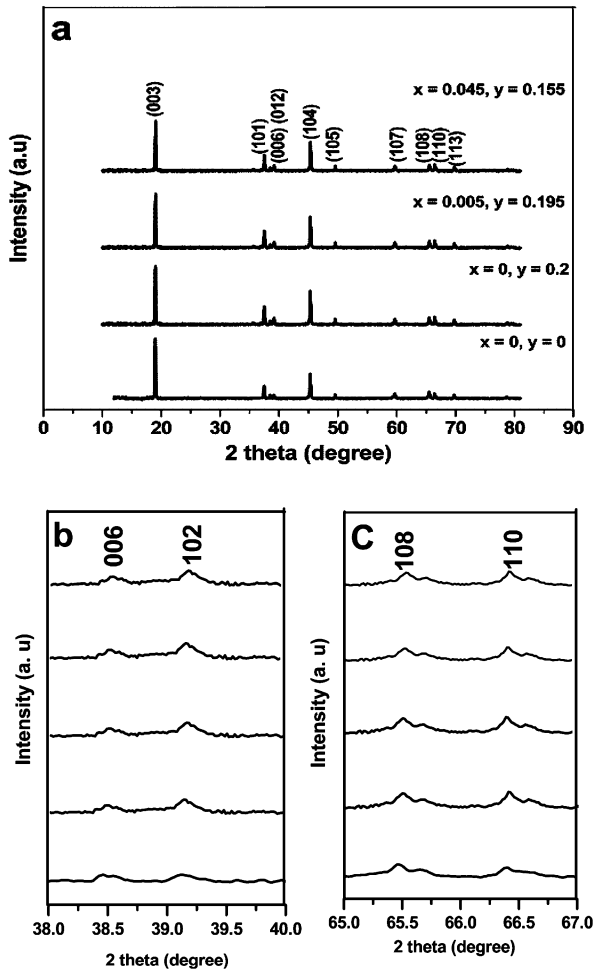

Figure 1. (a) XRD patterns of $LiMg_xCu_yCo_{1-x-y}O_2$, Magnified patterns of (b) (006) and (102) and (c) (108) and (110).

crystallites of 0.1−0.5 μm size. Particles synthesized by microwave method are smaller compared to other methods of synthesis, because the metal acetate precursors undergo slow hydrolysis during reaction in the initial heating process and produces small size particles. This kind of smaller size particles should exhibit good electrochemical activity during charge/discharge process.

Vibrational spectroscopy is one of the most useful techniques to investigate the local environment of the metal cations and surrounding ligands. Figure 3 shows the IR spectra of $LiMg_xCu_yCo_{1-x-y}O_2$ materials. The IR active modes of $LiCoO_2$ are $2A_{2u}$ and $2E_u$.[28] The symmetric stretching modes of Li−O located[29] at 269 cm^{-1} could not be recorded, because our instrument cannot be driven below 400 cm^{-1}. The frequency at 522 cm^{-1} corresponds to Li−O asymmetric stretching vibration, which shifts to higher value when doped with Cu and Mg.[30,31] The high frequency vibration at 596 cm^{-1} can be assigned to Co−O stretching motions.[32] The Cu−O and Mg−O vibrations are observed at 614 and 640 cm^{-1}.[33,34] The Co−O vibration of $LiCu_{0.2}Co_{0.8}O_2$ as well as Cu- and Mg-doped materials appear at 604−620 cm^{-1} conceal the Cu−O and Mg−O vibration because Cu (≤0.2) and Mg (≤0.05) concentrations are small. The absence of peak at 660 cm^{-1} indicates that spinel related phases have not formed in the synthesized materials. These results demonstrate that by doping, the local environment of lithium ions surrounded by

Table 1. Lattice Parameters of $LiMg_xCu_yCo_{1-x-y}O_2$ Materials

x, y	a (Å)	c (Å)	c/a	cell volume (Å)^3	$I_{003}/_{104}$	R	std deviation
0, 0	2.812	14.014	4.983	96.003	2.49	0.53	0. 0031
0, 0.2	2.815	14.068	4.997	96.103	1.49	0.41	0.0005
0.005, 0.195	2.814	14.062	4.997	96.098	1.32	0.39	0.0001
0.045, 0.155	2.815	14.052	4.991	96.078	1.34	0.49	0.0003

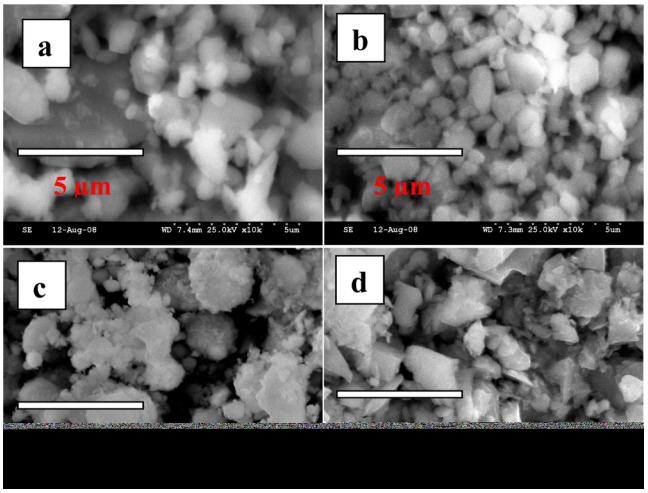

Figure 2. SEM images of $LiMg_xCu_yCo_{1-x-y}O_2$ (a) x, y = 0, 0; (b) x, y = 0, 0.2; (c) x, y = 0. 005, 0.195; (d) x, y = 0.045, 0.155.

Figure 3. IR spectra of $LiMg_xCu_yCo_{1-x-y}O_2$: (a) x, y = 0, 0; (b) x, y = 0, 0.2; (c) x, y = 0. 005, 0.195; (d) x, y = 0.045, 0.155.

oxygen ions does not get affected and only a slight broadening of the peaks is observed in the presence of dopants.

The vibration modes of $LiCoO_2$ having $R\bar{3}m$ space group are $A_{1g} + E_g + 2A_{2u} + 2E_u$ where A_{1g} and E_g modes are Raman active and $2A_{2u}$ and $2E_u$ are IR active. The Raman active modes[35,36] of A_{1g} and E_g are usually observed at 597 and 487 cm^{-1}. In Figure 4, two strong bands are observed at 595 and 485 cm^{-1} for $LiCoO_2$ as well as doped materials. In general, Raman modes are entirely due to oxygen atoms and the symmetry motions entail Co−O stretching and O−Co−O bending vibrations. The absence of vibrational bands at 440, 470, and 680 cm^{-1} implies that the spinel related phase Co_3O_4 is not present in the synthesized materials. Raman active modes of Cu−O bond[37] A_g and $2B_g$ are observed at 298, 330, and 602 cm^{-1}. The Raman bands of Mg−O bond[38] are seen at 595, 719, and 1096 cm^{-1}. In the present work, the Raman active modes of Cu−O (602 cm^{-1}) and Mg−O (595 cm^{-1}) can not be observed individually as the spectral band of Co−O masked this region. The higher frequency band of Mg−O bond observed at 725 cm^{-1} are in well agreement with reported work.[38] However, the lower frequency band of Cu−O could not be observed in the present work because of instrumental limitations.

Figure 4. Laser Raman spectra of $LiMg_xCu_yCo_{1-x-y}O_2$: (a) x, y = 0, 0; (b) x, y = 0, 0.2; (c) x, y = 0. 005, 0.195; (d) x, y = 0.045, 0.155.

To confirm the oxidation states of the metal cations present in the $LiMg_xCu_yCo_{1-x-y}O_2$ material, we carried out XPS studies (Figures 5 and 6). Figure 5 shows the survey spectra of $LiMg_xCu_yCo_{1-x-y}O_2$ materials. The characteristic binding energy of Mg2p is 50.8 eV, which ascertains the presence of Mg is in divalent state.[25] The Co2p bands are observed as splits at 779.3 eV for $Co2p_{3/2}$ and 794.9 eV for $Co2p_{1/2}$, which may

Figure 5. XPS survey spectra of $LiMg_xCu_yCo_{1-x-y}O_2$ materials.

dx.doi.org/10.1021/am300842x | ACS Appl. Mater. Interfaces 2012, 4, 4040−4046

Figure 6. XPS spectra of Mg2p, Cu2p, and Co2p lines.

be due to spin orbital interactions. These two bands imply that the Co is in trivalent state which is good agreement with previous works.[39−41] Two peaks are observed for Cu2p at 934.4 eV for $Cu2p_{3/2}$, and at 954.4 eV for $Cu2p_{1/2}$. The doublet peaks are separated by ∼20 eV and the satellite peaks are observed around ∼8 eV away from the main peaks. Similar satellite structure was observed in CuO, indicating that Cu ions are mostly divalent.[42] Further the calculated auger parameter for $Cu2p_{3/2}$ spectral line is 1852. eV (auger kinetic energy for $Cu2p_{3/2}$ line is 918.1 eV from the experiment) ascertains that Cu ions present in 2+ state which is in good agreement with reported literature.[43] The atom composition of the synthesized active materials are determined by using CasaXPS software (after correcting with respective elemental sensitivity factors) and listed in Table 2, which are almost matches with the actual composition.

Figure 7a presents the specific capacity vs potential curve of $LiMg_xCu_yCo_{1-x-y}O_2$ cathode materials cycled between the potential limits of 2.9−4.6 V at 0.2C rate. The first cycle discharge capacities are 120, 155, 208, and 193 mA h g^{-1} for (x, y = 0, 0), (x, y = 0, 0.2), (x, y = 0.005, 0.195), and (x, y = 0.045, 0.155) respectively. The discharge curves are very smooth and a sudden drop in voltage from 4.6 to 4.4 V is due to the increase in internal resistance which may be attributed to the inability of cathode to accept lithium ions (which are consumed in the formation of SEI) in the structure during the initial stages of discharge process.[44,45] The discharge capacity of the $LiCoO_2$ material is poor as compared to the doped ones because of the dissolution of Co^{4+} ion into the electrolyte resulting in structural deterioration of $LiCoO_2$ material during charge/discharge process. The Cu-doped $LiCoO_2$ exhibit good cycling performance as compared to the pristine $LiCoO_2$ material,

Table 2. Atom Percentages of $LiMg_xCu_yCo_{1-x-y}O_2$ Materials

name	position (eV)	area	sensitivity factor[a]	atom (%)
		$LiMg_{0.005}Cu_{0.195}Co_{0.8}O_2$		
Li1s	54. 7	222455	0.02	25
Mg2p	50. 8	1112.27	0.12	0.124
Cu2p	934. 4	28919.4	6.3	4.874
	954. 4	14459.3		
Co2p	779.4	118642.7	3.8	20
	794.9	59321.3		
O1s	529.9	444910.0	0.66	49.99
		$LiMg_{0.045}Cu_{0.155}Co_{0.8}O_2$		
Li1s	54. 7	227300.1	0.02	25
Mg2p	50. 8	10228.5	0.12	1.124
Cu2p	934. 3	23487.3	6.3	3.875
	954. 4	11743.6		
Co2p	779.4	121228.1	3.8	20.01
	794.9	60614.3		
O1s	529.9	454600.0	0.66	49.99

[a]Values collected from www.uksaf.org.

because of the increase in conductivity of $LiCoO_2$ material after doping with Cu, as reported earlier.[46] Cu and Mg doped $LiCoO_2$ material exhibits large discharge capacities of 208 (x = 0.005, 0.195) and 193 mA h g^{-1} (x = 0.045, 0.155) at 0.2C rate. After doping with Mg, the capacity increases around 50 mA h g^{-1} which may be due to the increased structural stability in the high voltage region during cycling, which is favorable for lithium intercalation and deintercalation due to the enlargement of c-lattice. The Mg^{2+} ions act as pillars (pillaring effect[7,47] of Mg^{2+} ions increase the structural stability) and protect the crumbling of CoO_2 interslab layers, enhancing the lithium ion

Figure 7. (a) Charge/discharge behavior of $LiMg_xCu_yCo_{1-x-y}O_2$ materials at 0.2*C* rate, (b) Cycling performance of $LiMg_xCu_yCo_{1-x-y}O_2$ materials at 0.2*C* rate, (c) charge/discharge curves of $LiMg_{0.005}Cu_{0.195}Co_{0.8}O_2$ at different *C* rate, (d) rate capability of $LiMg_{0.005}Cu_{0.195}Co_{0.8}O_2$ at different *C* rate over 90 cycles.

diffusions (it has similar ionic radii to that of Li^+ ions), which eventually increases the discharge capacity. Complete extraction of lithium ions from the tetrahedral site requires high potential (> 4.2 V) and the mixed doping avoids structural deterioration. Therefore, it is clear that the dopant Cu enhances conductivity and Mg provides structural stability to $LiCoO_2$, and delivers large discharge capacity at high voltage regions (4.6 V) as verified from impedance measurements (Figure 8).

Figure 7b depicts the cycling performance of the synthesized materials at 0.2*C* rate over the investigated 100 cycles. At the 100th cycle, the discharge capacities are 65, 130, 185, and 168 mA h g^{-1} corresponding to capacity retentions of 60, 84, 88.1, and 86.9% for the concentrations (x, y = 0, 0), (x, y = 0, 0.2), (x, y = 0.005, 0.195) and (x, y = 0.045, 0.155), respectively. It is interesting to note that the discharge capacities of the Cu- and Mg-doped $LiCoO_2$ materials are higher and the capacity fade is very minimal at high voltage and high discharge rates as compared to the previous reports.[48−52] The Cu and Mg doped materials exhibit good capacity retention even after 100 cycles, which may be due to positive effects of the dopant ions Mg^{2+} and Cu^{2+} on the electrode surface, which restrain Co^{4+} dissolution into the electrolyte solution during cycling. As the dopant ions form solid solution over the surface of active particles forming a coating layer (intermediate layer)[7,53] and thus preventing the dissolution of Co^{4+} ions in the electrolyte. This solid solution formed by dopant ions provide structural stability to active metal ions due to the pillaring effect of Mg^{2+} dopant ions,[54] eventually increasing the discharge capacity and minimizing capacity fading. Further, the dopants enlarge the lattice volume which is favorable for lithium intercalation and deintercalation as evidenced by XRD analysis The obtained discharge capacities and capacity retentions in the present work are comparable to that of $Li_4Ti_5O_{12}$-coated[55] $LiCoO_2$ electrodes in which the initial discharge capacity exhibited is ∼191 mA h g^{-1} when cycled between 2.9 and 4.5 V with a less irreversible capacity of 9 mA h g^{-1}. Therefore, the results suggest that Cu and Mg doping provide good structural stability to $LiCoO_2$ cathode materials and improved electrochemical behavior as reported in coating[55] of $LiCoO_2$

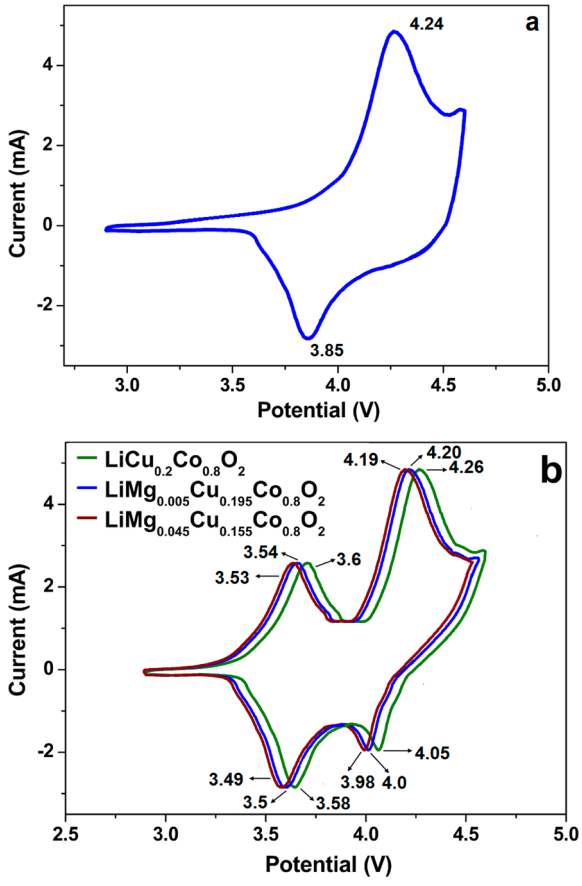

Figure 8. Cyclic Voltammogram of (a) $LiCoO_2$, (b) $LiMg_xCu_yCo_{1-x-y}O_2$ at the scan rate of 0.1 mV s^{-1}.

Lithium ion batteries require good rate capabilities for high power applications. This demands that the electrode can retain a large amount of its full capacity when discharged at high

dx.doi.org/10.1021/am300842x | ACS Appl. Mater. Interfaces 2012, 4, 4040−4046

current densities. For this purpose, we evaluated the coin cells cycled at different C−rates as shown in Figure 7c (for clarity, plots at 0.1, 0.5, 1, 2, 5, and 10C rates are presented). The discharge capacities are 230, 170, 140, 120, 80, and 50 mA h g^{-1} at 0.1, 0.5, 1, 2, 5, and 10*C* rates, respectively. It can be seen that the discharge capacity reduces with increase in current densities. The lowering of discharge capacities at higher current densities is due to the increase in cell polarization and internal resistance. The cycling performance of $LiMg_{0.005}Cu_{0.195}Co_{0.8}O_2$ at different *C*-rates, shown in Figure 7d, indicates that with increasing current rate the capacity fade also increases. Thus it is evident that $LiMg_{0.005}Cu_{0.195}Co_{0.8}O_2$ electrodes are suitable for cycling at moderate current densities to achieve stable cycling performance.

Figure 8 shows the cyclic voltammogram (CV) of $LiMg_xCu_yCo_{1-x-y}O_2$ cathode materials recorded between the potential limits of 2.9−4.6 V at 0.025 mV s^{-1}. The anodic peaks are observed at 4.26 and 3.58 V whereas the corresponding cathodic peaks are observed around 4.0 and 3.58 V, respectively. Normally, the oxidation and reduction peaks are observed at 3.95 and 3.8 V, respectively, for $LiCoO_2$ materials when CV was recorded upto 4.3 V.[5] In the present work, the oxidation peak obtained at 4.2 V is the characteristic peak of deintercalation of Li^+ ions corresponding to the oxidation of Co^{3+}/Co^{4+} ions with the intercalation process taking place at 4 V. The other redox pair (at 3.6 V and 3.58 V) may be ascribed to the redox event[56] of Cu^{2+}/Cu^+ Vs Li/Li^+. According to H. F. Wang et al.,[57] during charging, a transition from hexagonal phase [H] to monoclinic phase [M] occurs around 4.1 V, with further transformation to hexagonal phase [H] taking place around 4.2 V Vs Li/Li^+. As compared to bare $LiCoO_2$, we observed that doping with Cu and Mg improved reversibility of Li^+ ion characteristics due to shorter Li^+ ion diffusion pathway. The shifting of peak potential in the anodic as well as cathodic region may be attributed to the co−existence of hexagonal and monoclinic phases.

The improved performance of $LiMg_xCu_yCo_{1-x-y}O_2$ materials is further validated by electrochemical impedance spectroscopy analysis as shown in Figure 9. Typical Nyquist plots of the $LiMg_xCu_yCo_{0.8}O_2$ materials exhibit a semi circle in the high-frequency region and straight line in the low frequency region which is attributed to the diffusion of Li ion into the bulk of the electrode material (Warburg diffusion). After doping with Cu and Mg in the $LiCoO_2$, the charge transfer resistance (R_{ct}) markedly decreases which is associated with Cu and Mg dopants increasing the conductivity of the $LiCoO_2$ material. The lithium ion diffusion coefficient could be calculated by using the following equation[58]

$$D = \frac{R^2T^2}{2A^2n^4F^4C^2\sigma^2}$$

where *R* is the gas constant, *T* is the absolute temperature, *n* is the number of electrons per molecule oxidized, *A* is the surface area, *F* is the Faraday's constant, *C* is the concentration, *D* is the diffusion coefficient, and σ is the coefficient of Warburg impedance which can be obtained from the intersection of the straight line on the real axis.[59] It is equal to $(R_s + R_{ct} - 2\sigma^2C_{dl})$. The diffusion coefficients of $LiCoO_2$, $LiCu_{0.2}Co_{0.8}O_2$ and $LiMg_{0.005}Cu_{0.195}Co_{0.8}O_2$ are 1. 05 × 10^{-10}, 5. 02 × 10^{-9} and 3. 78 × 10^{-8} cm^2 s^{-1}, respectively. It is clear that the diffusion coefficient of $LiCoO_2$ is greatly enhanced by Cu and Mg dopants, suggesting that doping contributes to the enhancement of electrical conductivity, which improving the capacity of the Cu and Mg doped material.

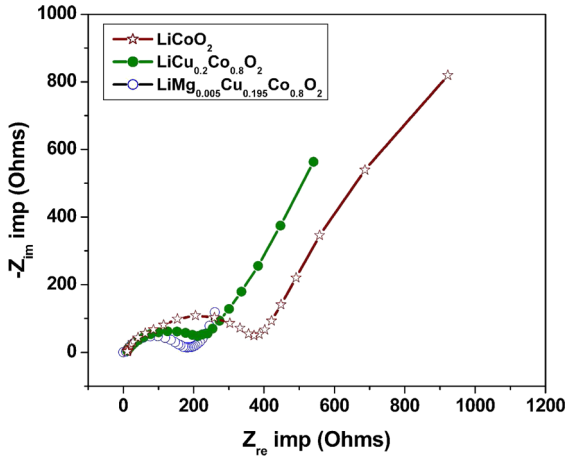

Figure 9. Nyquist plots of $LiMg_xCu_yCo_{0.8}O_2$ materials in the frequency range between 100 kHz and 5 mHz.

4. CONCLUSIONS

In conclusion, the microwave synthesis of $LiMg_xCu_yCo_{1-x-y}O_2$ cathode material yields smaller particle size and high cation ordering between Li and transition metal layers. Mg and Cu as mixed dopants provide enhanced conductivity and exhibit better structural stability in the high voltage regions up to 4.6 V. The cathode material $LiMg_{0.005}Cu_{0.195}Co_{0.8}O_2$ delivers the highest discharge capacity of 208 mA h g^{-1} at 0.2*C* rate retains 88% of the initial capacity even after 100 cycles. This cathode material performs well at high voltage as well as at high current rates.

AUTHOR INFORMATION

Corresponding Author

*E-mail: deepika_41@rediffmail.com. Fax: +91−4565−227779.

Notes

The authors declare no competing financial interest.

ACKNOWLEDGMENTS

The authors thank the Council of Scientific and Industrial Research (CSIR), India for support of this work under the project TAPSUN project of CSIR.

REFERENCES

(1) Toprakci, O.; Toprakci, H. A. K.; Ji, L.; Xu, G.; Lin, Z.; Zhang, X. *ACS Appl. Mater. Interfaces* **2012**, *4*, 1273−1280.
(2) Chen, J.; Graetz, J. *ACS Appl. Mater. Interfaces* **2011**, *3*, 1380−1384.
(3) Sun, Y. K.; Oh, I.; Kim, K. Y. *J. Mater. Chem.* **1997**, *7*, 1481−1486.
(4) Chen, Z.; Qin, Y.; Amine, K.; Sun, Y. K. *J. Mater. Chem.* **2010**, *20*, 7606−7612.
(5) Gopukumar, S.; Jeong, Y.; Kim, K. B. *Solid State Ionics* **2003**, *159*, 223−232.
(6) Zaheena, C. N.; Nithya, C.; Thirunakaran, R.; Sivashanmugam, A.; Gopukumar, S. *Electrochim. Acta* **2009**, *54*, 2877−2882.
(7) Kim, H. S.; Ko, T. K.; Na, B. K.; Cho, W.; Chao, B. W. *J. Power Sources* **2004**, *138*, 232−239.
(8) Liao, P. Y.; Duh, J. G.; Sheu, H. S. *J. Power Sources* **2008**, *183*, 766−770.

(9) Ma, X.; Wang, C.; Cheng, J.; Sun, J. *Solid State Ionics* **2007**, *178*, 125−129.
(10) Garcia, S. C; Couceriro, A. C.; Rodriguez, M. A.; Soulette, F.; Julien, C. *Solid State Ionics* **2003**, *156*, 15−26.
(11) Lala, S. M.; Montoro, L. A.; Lemos, V.; Abbate, M.; Rosolen, J. M. *Electrochim. Acta* **2005**, *51*, 7−13.
(12) Ghosh, P.; Mahanty, S.; Basu, R. N. *Electrochim. Acta* **2009**, *54*, 1654−1661.
(13) Cho, J.; Kim, Y. J.; Park, B. *Angew. Chem. Int. Ed.* **2001**, *40*, 3367−3367.
(14) Deepa, S.; Arvindhan, N. S.; Sugadev, C.; Tamilselvi, R.; Sakthivel, M.; Sivashanmugam, A.; Gopukumar, S. *Bull. Electrochem.* **1999**, *15*, 381−384.
(15) Zou, M.; Yoshio, M.; Gopukumar, S.; Yamaki, J. *Chem. Mater.* **2003**, *15*, 4699−4702.
(16) Saadoune, I.; Delmas, C. *J. Solid State Chem.* **1998**, *136*, 8−15.
(17) Elumalai, P.; Vasan, H. N.; Munichandraiah, N. *J. Power Sources* **2004**, *125*, 77−84.
(18) Luo, W.; Zhou, F.; Zhao, X.; Lu, Z.; Li, X.; Dahn, J. R. *Chem. Mater.* **2010**, *22*, 1164−1172.
(19) Tukamoto, H.; West, A. R. *J. Electrochem. Soc.* **1997**, *144*, 3164−3168.
(20) Eom, J.; Cho, J. *J. Electrochem. Soc.* **2008**, *155*, A201−A205.
(21) Madhavi, S.; Subba Rao, G. V.; Chowdari, B. V. R.; Li, S. F.Y. *Solid State Ionics* **2002**, *152− 153*, 199−205.
(22) Levasseur, S.; Menetrier, M.; Delmas, C. *Chem. Mater.* **2002**, *14*, 3584−3590.
(23) Mladenov, M.; Stoyanova, R.; Zhecheva, E.; Vassilev, S. *Electrochem. Commun.* **2001**, *3*, 410−416.
(24) Kim, H. J.; Jeong, Y. U.; Lee, J. H.; Kim, J. J. *J. Power Sources* **2006**, *159*, 233−236.
(25) Corneille, J. S.; He, J. W.; Goodman, D. W. *Surf. Sci.* **1994**, *306*, 269−278.
(26) Ohzuku, T.; Ueda, A.; Kouguchi, M. K. *J. Electrochem, Soc.* **1995**, *142*, 4033−4039.
(27) Makimura, Y.; Ohzuku, T. *J. Power Sources* **2003**, *119−121*, 156−160.
(28) Julien, C. M. *Solid State Ionics* **2000**, *136−137*, 887−896.
(29) Julien, C. M.; Massot, M. *J. Power Sources* **2003**, *119−121*, 743−748.
(30) Ohzuku, T.; Ueda, A.; Nagayama, M.; Iwakoshi, Y. *Electrochim. Acta* **1 993**, *38*, 1159−1167.
(31) Yi, T. F.; Zhu, Y. R. *Electrochim. Acta* **2008**, *53*, 3120−3126.
(32) Huang, W.; Frech, R. *Solid State Ionics* **1996**, *88−89*, 395−400.
(33) Sulochana, A.; Thirunakaran, R.; Sivashanmugam, A.; Gopukumar, S. *J. Electrochem. Soc.* **2008**, *155*, A206−A210.
(34) Balbuena, P. B.; Wang, Y. *Lithium-Ion Batteries: Solid−Electrolyte Interphase*; Imperial College Press: London, 2004; p 176.
(35) Inaba, M.; Iriyama, Y.; Ogumi, Z.; Todzuka, Y.; Tasaka, A. *J. Raman Spectrosc.* **1997**, *28*, 613−617.
(36) Julien, C.; Massot, M. *Phys. Chem. Chem. Phys.* **2002**, *4*, 4226−4235.
(37) Xu, J. F.; Ji, J.; Shen, Z. X.; Tang, S. H.; Ye, X. R.; Jia, D. Z.; Xin, X. Q. *J. Raman Spectrosc.* **1999**, *30*, 413−417.
(38) Schletcht, R. G.; Bockelmann, H. K. *Phys. Rev. Lett.* **1973**, *31*, 930−932.
(39) Balbuena, P.; Wang, Y., Eds; *Lithium-Ion Batteries: Solid Electrolyte Interphase*; Imperial College Press: London, 2004; p 185.
(40) Rao, M. C. *Optoelectron. Adv. Mater.−Rapid Commun.* **2011**, *5*, 651−654.
(41) Appapillai, A. T.; Mansour, A. N.; Cho, J.; Horn, Y. S. *Chem. Mater.* **2007**, *19*, 5748−5757.
(42) Fortunato, G.; Oswald, H. R.; Reller, A. *J. Mater. Chem.* **2001**, *11*, 905−911.
(43) Biesinger, M. C.; Lau, L. W. M.; Gerson, A. R.; Smart, R. St. C. *Appl. Surf. Sci.* **2010**, *257*, 887−898.
(44) Ramasamy, R. P.; White, R. E.; Popov, B. N. *J. Power Sources* **2005**, *141*, 298−306.
(45) Kang, S.; Abraham, D. P.; Yoon, W. S.; Nam, K. .; Yang, X. Q. *Electrochim. Acta* **2008**, *54*, 684−689.
(46) Nithya, C.; Thirunakaran, R.; Sivashanmugam, A.; Gopukumar, S. *J. Power Sources* **2011**, *196*, 6788−6793.
(47) Valanarasu, S.; Chandramohan, R.; Thirumalai, J.; Vijayan, T. A. *J. Sci. Res.* **2010**, *2*, 443−452.
(48) Kim, H.; Jeong, Y. K.; Lee, J. H.; Kim, J. J. *J. Power Sources* **2006**, *156*, 233−236.
(49) Needham, S. A.; Wang, G. X.; Liu, H. K.; Drozd, V. A.; Liu, R. S. *J. Power Sources* **2007**, *174*, 828−831.
(50) Xu, H. X.; Xie, S.; Zhang, C. P.; Chen, C. H. *J. Power Sources* **2005**, *148*, 90−94.
(51) Vasanthi, R.; Ruthmangani, I.; Selladurai, S. *Inorg. Chem. Commun.* **2005**, *6*, 953−957.
(52) Bai, Y.; Shi, H.; Wang, Z.; Chen, L. *J. Power Sources* **2007**, *167*, 504−509.
(53) Ohzuku, T.; Ueda, A. *J. Electrochem. Soc.* **1994**, *141*, 2972−2977.
(54) Pouillerie, C.; Croguennec, L.; Delmas, C. *Solid State Ionics* **2000**, *132*, 15−29.
(55) Yi, T. F.; Shu, J.; Wang, Y.; Xue, J.; Mang, J.; Yue, C. B.; Zhu, R. S. *Surf. Coat. Technol.* **2011**, *205*, 3885−3889.
(56) Cabellero, A.; Yusta, M. C.; Morales, J.; Pena, J. S.; Castellan, E. R. *Eur. J. Inorg. Chem.* **2006**, 1758−1764.
(57) Wang, H. F.; Jang, Y. I.; Huang, B. J.; Sadoway, D. R.; Chiang, J. M. *J. Electrochem. Soc.* **1999**, *146*, 473−480.
(58) Yang, K.; Deng, Z.; Suo, J. *J. Power Sources* **2012**, *201*, 274−279.
(59) Shi, M.; Chen, Z.; Sun, J. *Cem. Concr. Res.* **1999**, *29*, 1111−1115.